ELECTRONIC RESEARCH ARCHIVE
Volume **28**, Number **2**, June **2020**

doi:10.3934/era.2020061
pp. **1107–1121**

GENERATING GEOMETRIC BODY SHAPES WITH ELECTROMAGNETIC SOURCE SCATTERING TECHNIQUES

Youzi He[1], Bin Li[2], Tingting Sheng[3] and Xianchao Wang[4,5,*]

[1]Department of Mathematics, Hong Kong Baptist University
Kowloon, Hong Kong SAR, China
[2]School of Mathematics and Statistics
Qilu University of Technology (Shandong Academy of Sciences)
Jinan 250353, Shandong, China
[3]School of Economics, Changchun University of Finance and Economics
Changchun 130122, Jilin, China
[4]Department of Mathematics, City University of Hong Kong
Kowloon, Hong Kong SAR, China
[5]School of Astronautics, Harbin Institute of Technology
Harbin 150001, Heilongjiang, China

Abstract. In this paper, we are concerned with the three-dimensional (3D) geometric body shape generation with several well-selected characteristic values. Since 3D human shapes can be viewed as the support of the electromagnetic sources, we formulate a scheme to regenerate 3D human shapes by inverse scattering theory. With the help of vector spherical harmonics expansion of the magnetic far field pattern, we build on a smart one-to-one correspondence between the geometric body space and the multi-dimensional vector space that consists of all coefficients of the spherical vector wave function expansion of the magnetic far field pattern. Therefore, these coefficients can serve as the shape generator. For a collection of geometric body shapes, we obtain the inputs (characteristic values of the body shapes) and the outputs (the coefficients of the spherical vector wave function expansion of the corresponding magnetic far field patterns). Then, for any unknown body shape with the given characteristic set, we use the multivariate Lagrange interpolation to get the shape generator of this new shape. Finally, we get the reconstruction of this unknown shape by using the multiple-frequency Fourier method. Numerical examples of both whole body shapes and human head shapes verify the effectiveness of the proposed method.

1. **Introduction.** Recent advances in technology have enabled the construction of high-density point data sets that describe the surfaces of real objects, such as the human body. This development has brought an increasing number of important applications in modern industries, like mechanical engineering, film making, clothing industry and virtual game design. Moreover, the realism of virtual humans can be used in health and fitness research, including evaluation of body composition, study of nutritional disorders (obesity, coronary artery disease, metabolic arthritis and etc). All of the methods for capturing and processing three-dimensional (3D) human surface data could be mainly categorized into three types—silhouette-based

2020 *Mathematics Subject Classification.* Primary: 78A46, 78A25, 35R30.
Key words and phrases. Geometric body generation, electromagnetic sources scattering, multivariate Lagrange interpolation, multiple-frequency Fourier method.
* Corresponding author: Xianchao Wang.

methods, marker-based methods and measurement-based methods. When using the silhouette method [13], a silhouette of the whole human body is photographed on a reduced scale from different directions to obtain measurements of 3D geometric shapes by re-reading of two-dimensional (2D) forms, which can be extracted relatively robustly from images and they encode a great deal of information to recover 3D shapes. However, the performance of this method is limited due to artifacts such as shadow and noisy background segmentation. Marker-based body capture systems acquire the positions of the markers, which are attached to the surface of the body and create a complete surface mesh given the sparse marker positions [1]. While silhouette-based methods and marker-based methods are effective and visually convincing, these types of approaches need to take several measurements on every subject in the sample, which are costly, time consuming and labour intensive. Besides, these methods could easily become ineffective when the subjects wear heavy or baggy garments.

The above-mentioned defects of these methods motivate researchers to adopt simple and time-efficient measurement-based methods [12]. Using anthropometric landmarks, i.e. several well-selected features of the body shape as characteristic values is the usual way to model human body. Among the options of the characteristic values, the qualitative description of body shape such as body attributes (banana, pear, apple or hourglass) can reflect the overall characteristics of the body shape. And this kind of parameters can significantly reduce the number of characteristic values needed. The most relevant numerical values to these attributes is hip-to-waist ratio (HWR). Another parameter that can characterize body shape globally is body mass index (BMI), which can not be obtained from the silhouette-based or the marker-based data. Furthermore, it is obvious that such characteristic values are relatively insusceptible to articulation changes than those silhouettes measurements. By employing the appropriate parameters, one can determine the decent body shape uniquely. Recently, Li et al. [4] built a novel system, which borrows the source scattering and machine learning techniques to generate the desired geometric body shape by a couple of input characteristic values, such as height and relative weight.

In this paper, we consider to borrow the electromagnetic source scattering techniques to generate 3D human shapes. Our reconstruction scheme relies on the fact that we can view the body as the support of the electromagnetic source $\boldsymbol{J}$ satisfying the following time-harmonic Maxwell system

$$\begin{aligned} \nabla \times \boldsymbol{E} - \mathrm{i}\omega\mu_0 \boldsymbol{H} &= 0, \\ \nabla \times \boldsymbol{H} + \mathrm{i}\omega\varepsilon_0 \boldsymbol{E} &= \boldsymbol{J}, \end{aligned} \tag{1.1}$$

where $\mathrm{i} = \sqrt{-1}$ is the imaginary unit, $\boldsymbol{E}, \boldsymbol{H}$ are time-harmonic electromagnetic fields, $\omega > 0$ is the radial frequency, $\mu_0 > 0$ and $\varepsilon_0 > 0$ are magnetic permeability and electric permittivity constants of the isotropic homogeneous background medium, respectively. By the theory of source scattering, we can establish a smart one-to-one correspondence between the geometric body shape and the far-field pattern of the inverse source problem induced by the Maxwell system. With the help of the vector spherical harmonics expansion of the magnetic far field pattern, we can further build on a one-to-one correspondence between the geometric body space and the multi-dimensional vector space, which consists of all coefficients of the spherical vector wave function expansion of the magnetic far field pattern. Therefore, we could define these coefficients as the shape generator. For a collection of given

geometric body shapes, the inputs (several well-selected characteristic values of the given geometric body shapes) and the outputs (the coefficients of the spherical vector wave function expansion of the corresponding magnetic far field patterns) assemble the training data set. Then, we utilize these data to train the learning model. So, for any new unknown geometric body shape with the given characteristic set, we use the multivariate Lagrange interpolation to get the shape generator of this unknown shape. Next, with the help of the multiple-frequency Fourier method [14, 15, 16], we could finally obtain the reconstruction of this geometric body shape.

A pivotal idea in our method is that we view the 3D human shape as the support of the electromagnetic source. Therefore we could resort to electromagnetic source scattering techniques. For the electromagnetic waves, due to their relatively small wavelength compared with the wavelength of acoustic wave and because we can expect the optimum resolution to be around the half wavelength, our method is superior to most existing methods in terms of fineness. Moreover, unlike many other methods, which are based on non-Euclidean approximation and interpolation or function interpolation [4], our method only needs to deal with vector interpolation. This makes the proposed scheme easy to implement. Numerical examples of both the whole body shapes and the human head shapes illustrate the effectiveness and high-precision of our method.

The rest of the paper is organized as follows. In the next section, we give the definition of the geometric body shape space and the characteristic value space. In Section 3, we describe the multi-frequency direct and inverse electromagnetic source scattering problem. After that, we develop a novel scheme for geometric body shape generation in Section 4. We first introduce the notion—shape generator. Then we use the training dataset to train the learning model by multivariate Lagrange interpolation. Finally, the geometric body shape is reconstructed by the multiple-frequency Fourier method. In Section 5, we conduct two 3D experiments to illustrate the effectiveness and high-precision of the proposed method. In this paper, we use bold font to signify vectorial quantities (typically in 3D).

2. **Manifold theory.** In this section, we recall some elementary knowledge about the shape manifold theory, which will be used in our subsequent research.

Definition 2.1. Let U be a topological n-manifold with $n \in \mathbb{N}_+$ and $\Psi_U := \{\psi^p\}_{p\in\mathcal{P}}$ a set of characteristic values associated with U that are invariant under any isometry. Here, Ψ_U is said to be a characteristic set of U if it uniquely determines U, and vice versa.

Actually, the above definition includes much general geometric shape. In our study, we are exclusively consider cases in which U can be embedded into $\mathbb{R}^3$, as a bounded domain. However, this case is generally sufficient to embrace the human body shape as a specific example.

Obviously, more complex the geometric shape is, more characteristic values associated with it needed. For those complicated shapes, such as human body, the cardinality of the set of characteristic values may be infinite. However, for realistic reason, we always consider finite characteristic values for those complicated geometric shape. In our study, we consider the following space

$$\mathcal{S} := \mathcal{U} \times \mathcal{V}$$

where $\mathcal{U}$ is the space of all bounded domains in $\mathbb{R}^3$ and $\mathcal{V}$ is the N-dimensional vector space consisting of all characteristic values. By Definition 2.1, there is a one-to-one correspondence between the geometric shape and its characteristic set.

3. **Electromagnetic source scattering problem.** A critical idea in our method is that the 3D human shape can be regarded as the support of the electromagnetic source. So, in this section, we present some knowledge about the electromagnetic source scattering problem that are pertinent to our subsequent study. We assume the time-harmonic resultant electromagnetic field $\boldsymbol{E}, \boldsymbol{H}$ radiated from a electromagnetic source $\boldsymbol{J}$ is given by (1.1). Further, the behavior of an electromagnetic wave satisfies the Silver-Müller radiation condition

$$\lim_{|\boldsymbol{x}|\to+\infty} |\boldsymbol{x}|(\sqrt{\mu_0}\boldsymbol{H}\times\hat{\boldsymbol{x}}-\sqrt{\varepsilon_0}\boldsymbol{E})=0, \tag{3.1}$$

for all directions $\hat{\boldsymbol{x}}=\boldsymbol{x}/|\boldsymbol{x}|$ with $\boldsymbol{x}=(x_1,x_2,x_3)\in\mathbb{R}^3$. The wavenumber is defined by $k:=\omega\sqrt{\mu_0\varepsilon_0}$.

In this work, we will assume that the electromagnetic source $\boldsymbol{J}$ is a volume current that is supported in U, where $U\subset\mathbb{R}^3$ is a simply-connected bounded domain with a Lipschitz boundary ∂U. Since non-radiating sources produce no radiating field outside U, one can only recover the radiating part of the current distribution without any a prior knowledge. In order to formulate the one-to-one correspondence between tne electromagnetic field and the electromagnetic source, we assume that the electromagnetic source $\boldsymbol{J}$ only contains radiating sources and has the following form [6]

$$\boldsymbol{J}=\boldsymbol{p}f,$$

where

$$f=\begin{cases}1, & \text{in } U,\\ 0, & \text{otherwise},\end{cases} \tag{3.2}$$

and the polarization vector $\boldsymbol{p}$ is assumed to be known. Assume U is contained in a cube $D:=[-\alpha/2,\alpha/2]^3$, where $\alpha\in\mathbb{R}_+$ is independent of the wavenumber $k\in\mathbb{R}_+$. In this setting, determining the source $\boldsymbol{J}$ is equivalent to determining the manifold U.

Using the vectorial Green function, the radiating fields to the Maxwell system (1.1), (3.1) can be written as

$$\boldsymbol{E}(\boldsymbol{x})=\mathrm{i}\omega\mu_0\Big(\boldsymbol{I}+\frac{1}{k^2}\nabla\nabla\cdot\Big)\int_{\mathbb{R}^3}\Phi(\boldsymbol{x},\boldsymbol{y})\boldsymbol{J}(\boldsymbol{y})\mathrm{d}\boldsymbol{y}, \tag{3.3}$$

$$\boldsymbol{H}(\boldsymbol{x})=\nabla\times\int_{\mathbb{R}^3}\Phi(\boldsymbol{x},\boldsymbol{y})\boldsymbol{J}(\boldsymbol{y})\mathrm{d}\boldsymbol{y}, \tag{3.4}$$

where $\boldsymbol{I}$ is the 3×3 identity matrix and

$$\Phi(\boldsymbol{x},\boldsymbol{y})=\frac{\mathrm{e}^{\mathrm{i}k|\boldsymbol{x}-\boldsymbol{y}|}}{4\pi|\boldsymbol{x}-\boldsymbol{y}|},\quad \boldsymbol{x}\neq\boldsymbol{y},$$

is the fundamental solution to the Helmholtz equation. The radiating solution to the Maxwell system has the asymptotic form [2],

$$\boldsymbol{E}(\boldsymbol{x})=\frac{\mathrm{e}^{\mathrm{i}k|\boldsymbol{x}|}}{|\boldsymbol{x}|}\left\{\boldsymbol{E}_\infty(\hat{\boldsymbol{x}})+\mathcal{O}\Big(\frac{1}{|\boldsymbol{x}|}\Big)\right\},\ \boldsymbol{H}(\boldsymbol{x})=\frac{\mathrm{e}^{\mathrm{i}k|\boldsymbol{x}|}}{|\boldsymbol{x}|}\left\{\boldsymbol{H}_\infty(\hat{\boldsymbol{x}})+\mathcal{O}\Big(\frac{1}{|\boldsymbol{x}|}\Big)\right\},\ |\boldsymbol{x}|\to+\infty.$$

With the help of integral representations (3.3) and (3.4), we obtain

$$\boldsymbol{E}_\infty(\hat{\boldsymbol{x}}) = \frac{\mathrm{i}\omega\mu_0}{4\pi}\left(\boldsymbol{I} - \hat{\boldsymbol{x}}\hat{\boldsymbol{x}}^\top\right)\int_{\mathbb{R}^3} \mathrm{e}^{-\mathrm{i}k\hat{\boldsymbol{x}}\cdot\boldsymbol{y}}\boldsymbol{J}(\boldsymbol{y})\mathrm{d}\boldsymbol{y}, \tag{3.5}$$

$$\boldsymbol{H}_\infty(\hat{\boldsymbol{x}}) = \frac{\mathrm{i}k}{4\pi}\hat{\boldsymbol{x}}\times\int_{\mathbb{R}^3} \mathrm{e}^{-\mathrm{i}k\hat{\boldsymbol{x}}\cdot\boldsymbol{y}}\boldsymbol{J}(\boldsymbol{y})\mathrm{d}\boldsymbol{y}. \tag{3.6}$$

With the above formulation, the multi-frequency electromagnetic direct source problem and inverse source problem can be stated as follows:

Direct Problem. Given a fixed polarization vector $\boldsymbol{p} \in \mathbb{P}$, a finite set $\mathbb{K}$ of admissible wavenumbers, and the electromagnetic source $\boldsymbol{J} = \boldsymbol{p}f$, find a solution $\boldsymbol{E}, \boldsymbol{H}$ satisfying the Maxwell system (1.1), (3.1).

Inverse Problem. Given a fixed polarization vector $\boldsymbol{p} \in \mathbb{P}$ and a finite set $\mathbb{K}$ of admissible wavenumbers, recover the source $\boldsymbol{J} = \boldsymbol{p}f$ from the measured electric far-field data $\{\boldsymbol{E}_\infty(\hat{\boldsymbol{x}}, k; U)\}_{k\in\mathbb{K}}$ or the magnetic far-field data $\{\boldsymbol{H}_\infty(\hat{\boldsymbol{x}}, k; U)\}_{k\in\mathbb{K}}$. The definitions of $\mathbb{P}$ and $\mathbb{K}$ are given in the next section.

4. A scheme for geometric body generation.

Based on the sound theoretical basis for electromagnetic source scattering, we proceed to formulate a novel scheme, which can generate 3D human shapes with partial input parameters.

4.1. Shape generators by inverse source scattering.

In this section, we will bring in an important notion, shape generator, so we can establish the one-to-one correspondence between the geometric shape space and a finite dimensional vector space. For self-containment, we first give the definition of the finite set $\mathbb{K}$ of admissible wavenumbers, the corresponding observation direction set and the admissible polarization direction set.

Definition 4.1. Let λ be a sufficiently small positive constant, $N_1 \in \mathbb{N}$. Any wavenumber that belongs to the set $\mathbb{K}$ is defined by

$$k_{\boldsymbol{l}} := \begin{cases} \dfrac{2\pi}{\alpha}|\boldsymbol{l}|_\infty, & \boldsymbol{l} \in \mathbb{Z}^3 \setminus \{\boldsymbol{0}\},\ |\boldsymbol{l}|_\infty \le N_1, \\ \dfrac{2\pi}{\alpha}\lambda, & \boldsymbol{l} = \boldsymbol{0}. \end{cases}$$

The corresponding observation direction that consists in the set $\mathbb{X}$ is given by

$$\hat{\boldsymbol{x}}_{\boldsymbol{l}} := \begin{cases} \hat{\boldsymbol{l}}, & \boldsymbol{l} \in \mathbb{Z}^3 \setminus \{\boldsymbol{0}\},\ |\boldsymbol{l}|_\infty \le N_1, \\ (1,0,0)^\top, & \boldsymbol{l} = \boldsymbol{0}, \end{cases} \tag{4.1}$$

where $\hat{\boldsymbol{l}} = \boldsymbol{l}/|\boldsymbol{l}|$. Besides, the admissible set of polarization direction is defined by

$$\mathbb{P} := \{\boldsymbol{p} \in \mathbb{S}^2 | \boldsymbol{p} \times \hat{\boldsymbol{x}}_{\boldsymbol{l}} \neq 0\},$$

where $\mathbb{S}^2 := \{\boldsymbol{x} \in \mathbb{R}^3 :\ |\boldsymbol{x}| = 1\}$ is the unit sphere, and $\hat{\boldsymbol{x}}_{\boldsymbol{l}}$ is defined in (4.1).

According to Theorem 3.1 in [15] and the integral representations (3.5) and (3.6), we know that there is a one-to-one correspondence between the geometric body shape U and the electric far-field data $\{\boldsymbol{E}_\infty(\hat{\boldsymbol{x}}, k; U)\}_{k\in\mathbb{K}}$ or the magnetic far-field data $\{\boldsymbol{H}_\infty(\hat{\boldsymbol{x}}, k; U)\}_{k\in\mathbb{K}}$.

Next, we give the spherical vector wave function expansion of the magnetic far-field pattern. Let $\{Y_n^m(\hat{\boldsymbol{x}}) : m = -n, \cdots, n;\ n = 0, 1, 2, \cdots\}$ be the spherical harmonics. Then the vector spherical harmonics are

$$\boldsymbol{V}_n^m(\hat{\boldsymbol{x}}) = \frac{1}{\sqrt{n(n+1)}}\mathrm{Grad}Y_n^m(\hat{\boldsymbol{x}}), \quad \boldsymbol{W}_n^m(\hat{\boldsymbol{x}}) = \hat{\boldsymbol{x}} \times \boldsymbol{V}_n^m(\hat{\boldsymbol{x}}), \quad \hat{\boldsymbol{x}} \in \mathbb{S}^2.$$

Let $L_t^2(\mathbb{S}^2) := \{\boldsymbol{u} \in (L^2(\mathbb{S}^2))^3 \ | \boldsymbol{u} \cdot \boldsymbol{\nu} = 0 \text{ a.e. on } \mathbb{S}^2\}$ be the space of tangential L^2 vector fields on the unit sphere, where $\boldsymbol{\nu}$ is the unit outer normal vector on $\mathbb{S}^2$. The vector spherical harmonics $\boldsymbol{V}_n^m$ and $\boldsymbol{W}_n^m$ for $m = -n, \cdots, n;\ n = 1, 2, \cdots$, form a complete orthonormal system in $L_t^2(\mathbb{S}^2)$. Further, since $\boldsymbol{H}_\infty$ is analytic [2], there is the following expansion

$$\boldsymbol{H}_\infty = \sum_{n=1}^{\infty} \sum_{m=-n}^{n} \Big(a_{n,m} \boldsymbol{V}_n^m + b_{n,m} \boldsymbol{W}_n^m \Big),$$

with the coefficients

$$a_{n,m} = \int_{\mathbb{S}^2} \boldsymbol{H}_\infty \cdot \overline{\boldsymbol{V}_n^m} \mathrm{d}s, \quad b_{n,m} = \int_{\mathbb{S}^2} \boldsymbol{H}_\infty \cdot \overline{\boldsymbol{W}_n^m} \mathrm{d}s, \tag{4.2}$$

where the overline denotes the complex conjugate. In practical applications, the infinite series $\boldsymbol{H}_\infty$ always need to be truncated by

$$\boldsymbol{H}_{\infty,N_0} = \sum_{n=1}^{N_0} \sum_{m=-n}^{n} \Big(a_{n,m} \boldsymbol{V}_n^m + b_{n,m} \boldsymbol{W}_n^m \Big), \quad N_0 \in \mathbb{N}. \tag{4.3}$$

Remark 4.2. From the previous analysis, ignoring the negligible truncation errors, we have established a one-to-one correspondence between the geometric body space and the finite dimensional vector space that consists of coefficients $\{a_{n,m}, b_{n,m} : m = -n, \cdots, n; n = 1, \cdots, N_0; k \in \mathbb{K}\}$ of the spherical vector wave function expansion of the magnetic far-field pattern.

Hence, we could call such vector as the shape generator. We give the following formal definition.

Definition 4.3. For a simply-connected bounded geometric shape $U \subset \mathbb{R}^3$, the finite dimensional vector

$$(a_{n,m}(k;U), b_{n,m}(k;U) : m = -n, \cdots, n; n = 1, \cdots, N_0; k \in \mathbb{K})$$

is called the shape generator of U, where the elements $a_{n,m}(k;U), b_{n,m}(k;U) : m = -n, \cdots, n; n = 1, \cdots, N_0; k \in \mathbb{K}$ are defined by (4.2).

4.2. **Shape generator prediction using multivariate Lagrange interpolation.** After establishing the one-to-one correspondence between the geometric body space and the finite dimensional vector space, we actually obtain the one-to-one correspondence between two finite dimensional vector spaces, which contain the characteristic values of the geometric body shapes and the shape generators of the geometric body shapes, respectively. In this part, we introduce the approach, by which we obtain the shape generator of a unknown geometric body shape from the given characteristic values of this shape.

For a collection of the geometric body shapes $(U_s, \Psi_{U_s})_{s=1,\cdots,S}$, the shape generators are given by $\{(a_{n,m}(k;U), b_{n,m}(k;U) : m = -n, \cdots, n; n = 1, \cdots, N_0; k \in \mathbb{K})\}_{s=1,\cdots,S}$. We define the training dataset of geometric body shape generation as follows:

Definition 4.4. For each given geometric body shape U with N well-selected characteristic values $\{\psi^p(U)\}_{p=1,\cdots,N}$, we can get the shape generator $(a_{n,m}(k;U), b_{n,m}(k;U) : m = -n, \cdots, n; n = 1, \cdots, N_0; k \in \mathbb{K})$. A pair $\big(\{\psi^p(U)\}_{p=1,\cdots,N}, (a_{n,m}(k;U), b_{n,m}(k;U) : m = -n, \cdots, n; n = 1, \cdots, N_0; k \in \mathbb{K})\big)$ is called a training example, and the collective dataset $\big(\{\psi^p(U_s)\}_{p=1,\cdots,N}, (a_{n,m}(k;U_s), b_{n,m}(k;U_s)\ :$

$m=-n,\cdots,n; n=1,\cdots,N_0; k\in\mathbb{K})\big)_{s=1,\cdots,S}$ is called a training dataset. Here, N well-selected characteristic values $\{\psi^p(U)\}_{p=1,\cdots,N}$ is the input, the shape generator $(a_{n,m}(k;U), b_{n,m}(k;U) : m=-n,\cdots,n; n=1,\cdots,N_0; k\in\mathbb{K})$ is the output.

The training dataset consists of a collection of geometric body shapes with their characteristic values and the corresponding shape generators, which can be calculated before training. Here, we aim to establish a learning model $F:\mathbb{R}^N\to\mathbb{C}^{2N_0(N_0+2)(N_1+1)}$ that maps the characteristic values of the geometric body shapes to the corresponding shape generators. Due to the pairwise independence of the Fourier coefficients $\{a_{n,m}(k;U), b_{n,m}(k;U) : m=-n,\cdots,n; n=1,\cdots,N_0\}_{k\in\mathbb{K}}$ and because the real parts and the imaginary parts of these coefficients do not affect each other, we build $4N_0(N_0+2)(N_1+1)$ learning models

$$\begin{aligned}&\mathrm{Re}a^{(k)}_{n,m}:=F^{(k)}_{1,n,m}(\psi^1,\cdots,\psi^N),\quad \mathrm{Im}a^{(k)}_{n,m}:=F^{(k)}_{2,n,m}(\psi^1,\cdots,\psi^N),\\&\mathrm{Re}b^{(k)}_{n,m}:=F^{(k)}_{3,n,m}(\psi^1,\cdots,\psi^N),\quad \mathrm{Im}b^{(k)}_{n,m}:=F^{(k)}_{4,n,m}(\psi^1,\cdots,\psi^N),\end{aligned}$$

respectively. Without loss of generality, we give the elaborate description of one learning model construction as following.

Let $F^{(\frac{2\pi}{a})}_{1,1,-1}(\psi^1,\cdots,\psi^N)$ be an $N-$variable multinomial function of degree q, i.e.,

$$F^{(\frac{2\pi}{a})}_{1,1,-1}(\psi^1,\cdots,\psi^N)=\sum_{\boldsymbol{e}_j\cdot\mathbf{1}\le q}\beta_{\boldsymbol{e}_j}\Psi^{\boldsymbol{e}_j},$$

where the $\beta_{\boldsymbol{e}_j}$ are the coefficients in $F^{(\frac{2\pi}{a})}_{1,1,-1}$, $\Psi=(\psi^1,\cdots,\psi^N)$ is the N-tuple of independent variables of $F^{(\frac{2\pi}{a})}_{1,1,-1}$, $\boldsymbol{e}_j=(e_{1j},\cdots,e_{Nj})$ is an exponent vector with nonnegative integer entries consisting of an ordered partition of an integer between 0 and q inclusive, $\boldsymbol{e}_j\cdot\mathbf{1}:=\sum\limits_{r=1}^{N}e_{rj}$ is the vector dot product, $\Psi^{\boldsymbol{e}_j}:=\prod\limits_{r=1}^{N}(\psi^r)^{e_{rj}}$. As there are $\binom{q+N}{q}=S$ terms in $F^{(\frac{2\pi}{a})}_{1,1,-1}$, the training dataset should consist of S distinct bodies, which corresponds to S distinct points $(\psi^1_i,\cdots,\psi^N_i,\mathrm{Re}a^{(\frac{2\pi}{a})}_{1,-1,i})\in\mathbb{R}^{N+1}, 1\le i\le S, \mathrm{Re}a^{(\frac{2\pi}{a})}_{1,-1,i}=F^{(\frac{2\pi}{a})}_{1,1,-1}(\psi^1_i,\cdots,\psi^N_i)$, for $F^{(\frac{2\pi}{a})}_{1,1,-1}$ to be uniquely defined. Following the idea of multivariate Lagrange interpolation [11], we wish to write $F^{(\frac{2\pi}{a})}_{1,1,-1}=\sum\limits_{i=1}^{S}\mathrm{Re}a^{(\frac{2\pi}{a})}_{1,-1,i}l_i(\Psi)$, where $l_i(\Psi)$ is a multinomial function w.r.t the independent variables $\psi^1,\cdots,\psi^N$ with the property that when $\Psi=\Psi_i$, i.e. $(\psi^1,\cdots,\psi^N)=(\psi^1_i,\cdots,\psi^N_i)$, then $l_i(\Psi_i)=1$ and $l_j(\Psi_i)=0(j\ne i)$. Thus, we consider the system $\mathrm{Re}a^{(\frac{2\pi}{a})}_{1,-1,i}=\sum\limits_{\boldsymbol{e}_j\cdot\mathbf{1}\le q}\beta_{\boldsymbol{e}_j}\Psi_i^{\boldsymbol{e}_j}$, where $\Psi_i^{\boldsymbol{e}_j}:=\prod\limits_{r=1}^{N}(\psi^r_i)^{e_{rj}}$, $1\le i\le S$. Then, we can construct the sample matrix $A=[\Psi_i^{\boldsymbol{e}_j}]$:

$$A=\begin{bmatrix}\Psi_1^{\boldsymbol{e}_1}&\cdots&\Psi_1^{\boldsymbol{e}_S}\\ \vdots&&\vdots\\ \Psi_i^{\boldsymbol{e}_1}&\cdots&\Psi_i^{\boldsymbol{e}_S}\\ \vdots&&\vdots\\ \Psi_S^{\boldsymbol{e}_1}&\cdots&\Psi_S^{\boldsymbol{e}_S}\end{bmatrix}.$$

Since $F^{(\frac{2\pi}{a})}_{1,1,-1}$ is unique if and only if its sample matrix is nonsingular, we assume $\det(A)\ne 0$. Further, we substitute Ψ for Ψ_i in A, this gives the following matrix

$A_i(\Psi)$:

$$A_i(\Psi) = \begin{bmatrix} \Psi_1^{\boldsymbol{e}_1} & \cdots & \Psi_1^{\boldsymbol{e}_S} \\ \vdots & & \vdots \\ \Psi^{\boldsymbol{e}_1} & \cdots & \Psi^{\boldsymbol{e}_S} \\ \vdots & & \vdots \\ \Psi_S^{\boldsymbol{e}_1} & \cdots & \Psi_S^{\boldsymbol{e}_S} \end{bmatrix} \leftarrow i^{\text{th}} \text{ row}.$$

Obviously, $l_i(\Psi) := \det(A_i(\Psi))/\det(A)$ satisfies $l_i(\Psi_i) = 1$ and $l_j(\Psi_i) = 0 (j \neq i)$. Hence,

$$F_{1,1,-1}^{(\frac{2\pi}{a})} = \sum_{i=1}^{S} \mathrm{Re} a_{1,-1,i}^{(\frac{2\pi}{a})} \frac{\det(A_i(\Psi))}{\det(A)}.$$

Following the same steps, we can get similar Lagrange interpolation expressions of $F_{1,n,m}^{(k)}$, $F_{2,n,m}^{(k)}$, $F_{3,n,m}^{(k)}$, $F_{4,n,m}^{(k)}$: $m = -n, \cdots, n; n = 1, \cdots, N_0; k \in \mathbb{K}$.

Until now, learning models have been established. For a new unknown geometric body shape U_{new} with given characteristic set $\Psi_{U_{new}}$, we could use the previous established model to get the approximate new shape generators $(a_{n,m}(k; U_{new}), b_{n,m}(k; U_{new}) : m = -n, \cdots, n; n = 1, \cdots, N_0; k \in \mathbb{K})$.

4.3. **Shape reconstruction with multiple-frequency Fourier method.** With the help of previous results, we can use the multiple-frequency Fourier method [15] to reconstruct the unknown shape U_{new} with the approximate shape generator $(a_{n,m}(k; U_{new}), b_{n,m}(k; U_{new}) : m = -n, \cdots, n; n = 1, \cdots, N_0; k \in \mathbb{K})$. We would like to mention in passing some relevant references [3, 5, 7, 10, 9, 8, 17, 18, 19] on the uniqueness and stability issues for inverse scattering problems that can provide the theoretical basis for the shape reconstruction in this subsection.

Firstly, we recall the Fourier basis functions

$$\phi_{\boldsymbol{l}}(\boldsymbol{x}) = \exp\left(\mathrm{i}\frac{2\pi}{\alpha}\boldsymbol{l} \cdot \boldsymbol{x}\right), \ \boldsymbol{l} \in \mathbb{Z}^3, \boldsymbol{x} \in \mathbb{R}^3. \tag{4.4}$$

The Fourier expansion of the electric current density $\boldsymbol{J}$ is

$$\boldsymbol{J} = \boldsymbol{p}f = \boldsymbol{p} \sum_{\boldsymbol{l} \in \mathbb{Z}^3} \hat{f}_{\boldsymbol{l}} \phi_{\boldsymbol{l}},$$

where the Fourier coefficients are given by

$$\hat{f}_{\boldsymbol{l}} = \frac{1}{\alpha^3} \int_D f(\boldsymbol{x}) \overline{\phi_{\boldsymbol{l}}(\boldsymbol{x})} \mathrm{d}\boldsymbol{x}.$$

By Definition 4.1, the Fourier basis functions (4.4) can be rewritten as

$$\phi_{\boldsymbol{l}}(\boldsymbol{x}) = \exp\big(\mathrm{i}k_{\boldsymbol{l}}\hat{\boldsymbol{l}} \cdot \boldsymbol{x}\big), \ \boldsymbol{l} \in \mathbb{Z}^3, \boldsymbol{x} \in \mathbb{R}^3.$$

For every $\boldsymbol{l} \in \mathbb{Z}^3 \backslash \{\boldsymbol{0}\}$, there is

$$\hat{f}_{\boldsymbol{l}} = \frac{4\pi \hat{\boldsymbol{x}}_{\boldsymbol{l}} \times \boldsymbol{p} \cdot \widetilde{\boldsymbol{H}}_\infty(\hat{\boldsymbol{x}}_{\boldsymbol{l}}, k_{\boldsymbol{l}}; U_{new})}{\mathrm{i}k_{\boldsymbol{l}}\alpha^3 |\hat{\boldsymbol{x}}_{\boldsymbol{l}} \times \boldsymbol{p}|^2}. \tag{4.5}$$

For $\boldsymbol{l} = \boldsymbol{0}$, we have

$$\begin{aligned} \hat{f}_{\boldsymbol{0}} = \frac{\lambda\pi}{\alpha^3 \sin\lambda\pi} \Bigg(& \frac{4\pi \hat{\boldsymbol{x}}_{\boldsymbol{0}} \times \boldsymbol{p} \cdot \widetilde{\boldsymbol{H}}_\infty(\hat{\boldsymbol{x}}_{\boldsymbol{0}}, k_{\boldsymbol{0}}; U_{new})}{\mathrm{i}k_{\boldsymbol{0}} |\hat{\boldsymbol{x}}_{\boldsymbol{0}} \times \boldsymbol{p}|^2} \\ & - \sum_{\boldsymbol{l} \in \mathbb{Z}^3 \backslash \{\boldsymbol{0}\}} \hat{f}_{\boldsymbol{l}} \int_D \exp\big(\mathrm{i}(k_{\boldsymbol{l}}\hat{\boldsymbol{l}} - k_{\boldsymbol{0}}\hat{\boldsymbol{x}}_{\boldsymbol{0}}) \cdot \boldsymbol{y}\big) \mathrm{d}\boldsymbol{y} \Bigg). \end{aligned} \tag{4.6}$$

All $k_{\boldsymbol{l}}, \hat{\boldsymbol{x}}_{\boldsymbol{l}}$ above come from Definition 4.1. For an appropriate $N_1 \in \mathbb{N}$ [15], $\boldsymbol{J}$ can be approximated by

$$\boldsymbol{J}_{N_1} = \boldsymbol{p} \sum_{|\boldsymbol{l}|_\infty \le N_1} \hat{f}_{\boldsymbol{l}} \phi_{\boldsymbol{l}}, \tag{4.7}$$

where $\hat{f}_{\boldsymbol{0}}$ could be approximately represented by

$$\begin{aligned} \hat{f}_{\boldsymbol{0}} \approx \frac{\lambda\pi}{\alpha^3 \sin\lambda\pi} \Bigg(& \frac{4\pi \hat{\boldsymbol{x}}_{\boldsymbol{0}} \times \boldsymbol{p} \cdot \widetilde{\boldsymbol{H}}_\infty(\hat{\boldsymbol{x}}_{\boldsymbol{0}}, k_{\boldsymbol{0}}; U_{new})}{\mathrm{i} k_{\boldsymbol{0}} |\hat{\boldsymbol{x}}_{\boldsymbol{0}} \times \boldsymbol{p}|^2} \\ & - \sum_{1 \le |\boldsymbol{l}|_\infty \le N_1} \hat{f}_{\boldsymbol{l}} \int_D \exp\big(\mathrm{i}(k_{\boldsymbol{l}} \hat{\boldsymbol{l}} - k_{\boldsymbol{0}} \hat{\boldsymbol{x}}_{\boldsymbol{0}}) \cdot \boldsymbol{y}\big) \mathrm{d}\boldsymbol{y} \Bigg). \end{aligned} \tag{4.8}$$

4.4. **Shape reconstruction scheme.** With the above preparations, we are ready to formulate the geometric body shape regeneration scheme in Algorithm I as follows.

Algorithm I: Geometric body shape regeneration scheme

Step 1	Select the parameters N_0, λ, N_1, the admissible wavenumber set $\mathbb{K}$ and the admissible observation direction set $\mathbb{X}$.
Step 2	For the given $\{U_s; \{\psi^p(U_s)\}_{p=1,\cdots,N}\}_{s=1,\cdots,S}$, solve the direct problem (1.1), (3.1) to get $\{\boldsymbol{H}_\infty(\hat{\boldsymbol{x}}, k; U_s)\}_{k\in\mathbb{K}, s=1,\cdots,S}$ and compute the corresponding coefficients $\{a_{n,m}(k;U_s), b_{n,m}(k;U_s) : m = -n,\cdots,n; n = 1,\cdots,N_0\}_{k\in\mathbb{K}, s=1,\cdots,S}$.
Step 3	Use the training dataset $\big(\{\psi^p(U_s)\}_{p=1,\cdots,N}, (a_{n,m}(k;U_s), b_{n,m}(k;U_s) : m = -n,\cdots,n; n = 1,\cdots,N_0; k \in \mathbb{K})\big)_{s=1,\cdots,S}$ to get Lagrange interpolation expressions $F^{(k)}_{1,n,m}$, $F^{(k)}_{2,n,m}$, $F^{(k)}_{3,n,m}$, $F^{(k)}_{4,n,m}$: $m = -n,\cdots,n; n = 1,\cdots,N_0; k \in \mathbb{K}$.
Step 4	For a new characteristic set $\{\psi^p(U_{new})\}_{p=1,\cdots,N}$, obtain the new shape generator $(a_{n,m}(k;U_{new}), b_{n,m}(k;U_{new}) : m = -n,\cdots,n; n = 1,\cdots,N_0; k \in \mathbb{K})$ with the help of the multivariate Lagrange interpolation, then get the approximate new magnetic far-field pattern $\{\widetilde{\boldsymbol{H}}_\infty(\hat{\boldsymbol{x}}, k; U_{new})\}_{k\in\mathbb{K}}$.
Step 5	Compute the Fourier coefficients $\hat{f}_{\boldsymbol{l}}$ for $|\boldsymbol{l}|_\infty \le N_1$ by (4.5) and (4.8).
Step 6	Select the sampling mesh $\mathcal{T}_h$ in the region D. For each sampling point $z_j \in \mathcal{T}_h$, calculate the functional $\boldsymbol{J}_{N_1}$ defined by (4.7), then U_{new} is got as the support of $\boldsymbol{J}_{N_1}$.

5. **Numerical examples.** In this section, we conduct some numerical experiments to illustrate the effectiveness of our shape regeneration method.

First, for each given shape U_s, we obtain the magnetic data $\boldsymbol{H}(\boldsymbol{x}, k; U_s)$ by solving the direct problem of (1.1). In order to avoid the inverse crime, the quadratic finite elements are used on a truncated spherical domain enclosed by a perfectly matched layer (PML), where the mesh of the forward solver is successively refined till the relative error of the successive artificial radiated data is below 0.1%. Then the synthetic magnetic far-field data $\{\boldsymbol{H}_\infty(\hat{\boldsymbol{x}}, k; U_s)\}_{k\in\mathbb{K}}$ are generated by applying the Kirchhoff integral formula to the radiated data. Thus, the shape generator $(a_{n,m}(k;U_s), b_{n,m}(k;U_s) : m = -n,\cdots,n; n = 1,\cdots,N_0; k \in \mathbb{K})$ is generated by

equation (4.2). It is remarked that we use an open source system Meshlab for processing and editing 3D triangular meshes.

Next, we present the implementation of multivariate Lagrange interpolation. Given the characteristic values $\{\psi^p(U_s)\}_{p=1,\cdots,N}$ and shape generator $(a_{n,m}(k;U_s), b_{n,m}(k;U_s) : m=-n,\cdots,n; n=1,\cdots,N_0; k\in\mathbb{K})$, the training dataset is given by

$$\left\{\{\psi^p(U_s)\}_{p=1}^N; (a_{n,m}(k;U_s), b_{n,m}(k;U_s): m=-n,\cdots,n; n=1,\cdots,N_0; k\in\mathbb{K})\right\}_{s=1}^S.$$

Here the input datum and the output datum are defined by

$$z_s = \{\psi^p(U_s)\}_{p=1}^N \in \mathbb{R}^N,$$
$$y_s = \{a_{n,m}(k;U_s), b_{n,m}(k;U_s)\}_{m=-n,\cdots,n;n=1,\cdots,N_0;k\in\mathbb{K}} \in \mathbb{C}^{2N_0(N_0+2)(N_1+1)}.$$

Therefore, we establish the mapping from the characteristic set to the shape generator. Moreover, for each wavenumber k_j, $j=1,2,\cdots,N_1+1$, we use multivariate Lagrange interpolation to obtain the shape generator $(a_{n,m}(k_j;U_{new}), b_{n,m}(k_j;U_{new}) : m=-n,\cdots,n; n=1,\cdots,N_0)$ with the new given characteristic set $\{\psi^p(U_{new})\}_{p=1}^N$.

Finally, we specify details of reconstructing the geometry body shape. As discussed above, reconstructing the geometry body shape is equal to reconstructing the electromagnetic source function $\boldsymbol{J}$. Based on the predicted shape generator $(a_{n,m}(k_j;U_{new}), b_{n,m}(k_j;U_{new}) : m=-n,\cdots,n; n=1,\cdots,N_0; j=1,\cdots,N_1+1)$, one can deduce the magnetic far-field data $\{\boldsymbol{H}_\infty(\hat{\boldsymbol{x}},k_j;U_{new}) : j=1,\cdots,N_1+1\}$ by (4.3). In the discrete formula, the domain D is divided into a uniform mesh with size $100\times100\times100$ in three dimensions. Furthermore, the approximated Fourier series $\hat{f}_{\boldsymbol{l}}$ are computed at the mesh nodes $\mathcal{T}_j$, $j=1,\cdots,100^3$ by (4.5) and (4.6). Thus, the geometry body shape U_{new} is approximated by the boundary of the imaging results $\boldsymbol{J}$, i.e., the support domain of the function f defined in (3.2).

In the following examples, the parameters are given by $N_0=10$, $N_1=20$, $\lambda=10^{-3}$ and the number of training dataset is given by $S=495$. In addition, the polarization direction is given by $\boldsymbol{p}=[\sqrt{5}/3,-1/3,\sqrt{3}/3]$.

Example 5.1. In the first example, we aim to reconstruct a 3D whole human body shape. The training dataset consists of 495 shapes of children which are generated randomly by the MakeHuman software [20]. In this experiment, the characteristic values of body are defined by default values of a standard three years children body for the MakeHuman software. Here, we consider changing four characteristic values, i.e., weight, muscle, scale horizontally and scale vertically of the body. To simplify, we use relative characteristic values, where the relative weight and muscle are from 50% to 150%, and the relative scale horizontally and scale vertically are from 80% to 120%. Some human body shapes in the training dataset are presented in Figure 1. We set $\alpha=1$ and choose a set of test dataset that is not covered by the training dataset, where the relative weight is 95%, relative weight is 105%, relative scale horizontally is 90% and relative scale horizontally 85%. Figure 2 shows the exact and the reconstructed body shape with the given characteristic values. It is clear that the reconstructed result is generally close to the exact body shape though the details are not well recovered. This result is as expected because we only select a few general characteristic values to determine the body shape. On the whole, the result shows that the proposed method is effective to predict the 3D human body shape.

Example 5.2. In this example, we would like to extract some more detailed feature values so that we could reconstruct details on the human body shape. Here, we

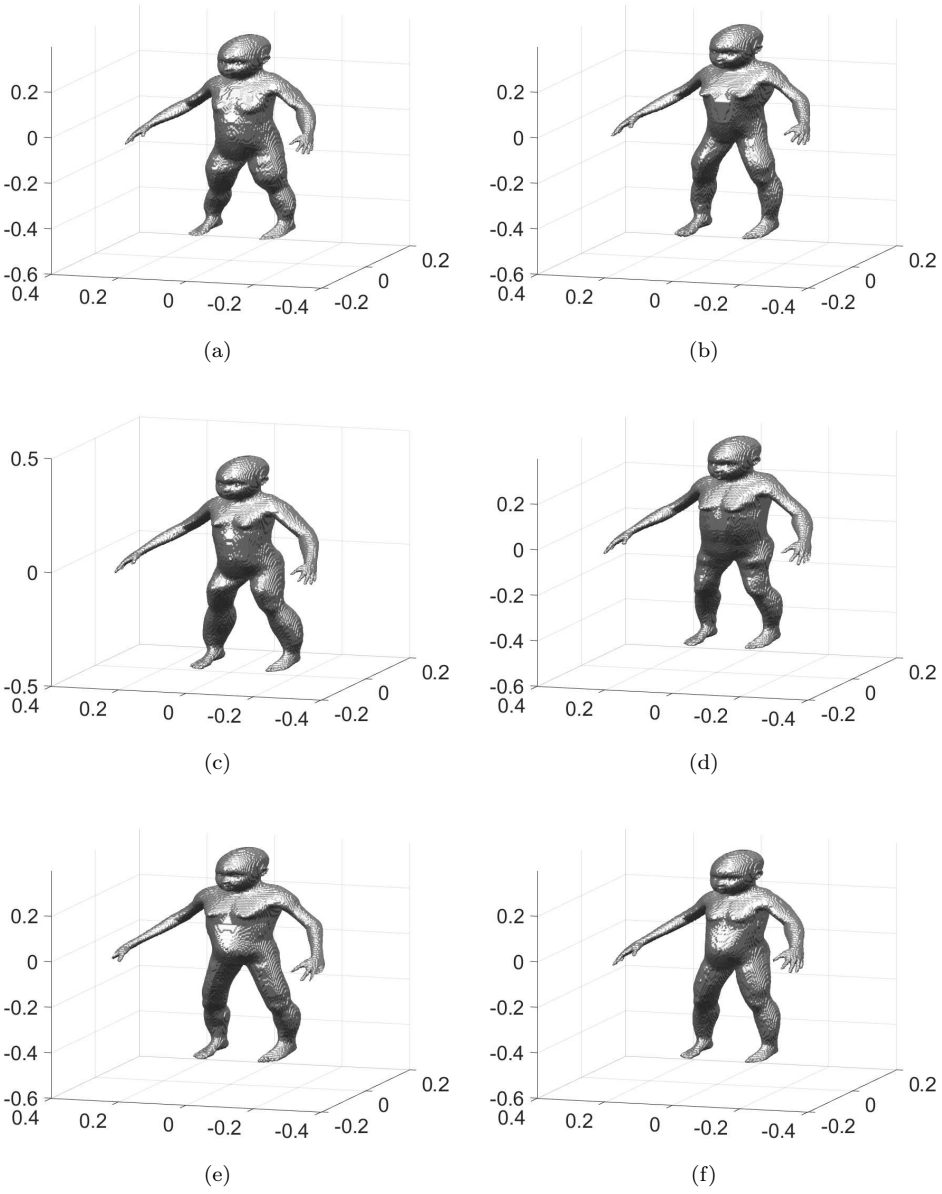

FIGURE 1. Isosurface plots of some random training body data with different characteristic values.

consider reconstructing the 3D human head shape and devote to determining the details of the head. The training dataset consists of 495 human heads which are also generated randomly by the MakeHuman software. In this experiment, the characteristic values of head are defined by default values of a standard grown-up body for the MakeHuman software. Here, we just consider changing the four major characteristic values, i.e., age, head fat, angle of the face and scale depth

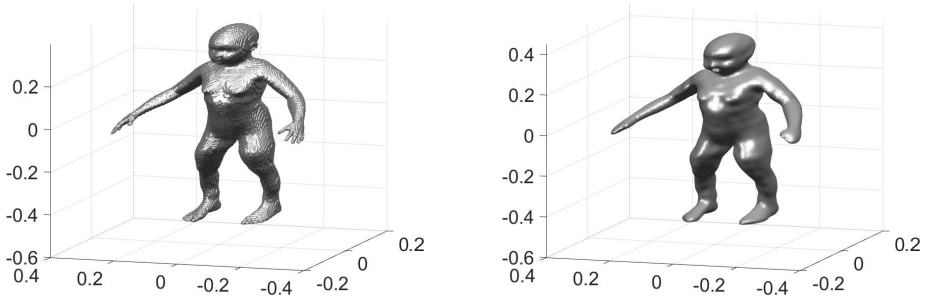

(a) (b)

FIGURE 2. Isosurface plots of the exact and reconstucted body shapes. (a) The exact child body, (b) the reonstucted child body with the given characteristic values.

of parietal side. For convenience of calculations, we also use relative characteristic values, where the relative values are from 75% to 125%. Figure 3 presents some human head shapes of the training dataset. We set $\alpha = 0.3$ and choose a group of characteristic values that is not covered by the training dataset, where the relative age is 123%, relative head fat is 110%, relative scale horizontally is 95% and relative scale depth of parietal side is 115%. Figure 4 shows the exact and the predicted head shapes with the given four characteristic values. This example confirms the effectiveness of our method when dealing with details on body shapes.

Acknowledgments. The authors would like to thank Professor Hongyu Liu of City University of Hong Kong for proposing this research as well as for providing many helpful discussions during the completion of this paper. The work of Bin Li was supported by the Development Plan of Young Innovation Team in Colleges and Universities of Shandong Province under Grant 2019KJN011. The work of Xianchao Wang was supported by the Hong Kong Scholars Program grant under No. XJ2019005 and the NSFC grant under No. 11971133.

REFERENCES

[1] D. Anguelov, P. Srinivasan, D. Koller, S. Thrun, J. Rodgers and J. Davis, SCAPE: Shape completion and animation of people, *ACM Transactions on Graphics (TOG)*, **24** (2005), 408–416.

[2] D. Colton and R. Kress, *Inverse Acoustic and Electromagnetic Scattering Theory*, Applied Mathematical Sciences, Vol. 93. Springer-Verlag, Berlin, 1998.

[3] J. Li, H. Liu, Z. Shang and H. Sun, Two single-shot methods for locating multiple electromagnetic scatterers, *SIAM J. Appl. Math.*, **73** (2013), 1721–1746.

[4] J. Li, H. Liu, W.-Y. Tsui and X. Wang, An inverse scattering approach for geometric body generation: A machine learning perspective, *Mathematics in Engineering*, **1** (2019), 800–823.

[5] J. Li, H. Liu and J. Zou, Locating multiple multiscale acoustic scatterers, *Multiscale Model. Simul.*, **12** (2014), 927–952.

[6] I. V. Lindell, TE/TM decomposition of electromagnetic sources, *IEEE Trans. Antennas and Propagation*, **36** (1988), 1382–1388.

[7] H. Liu, A global uniqueness for formally determined inverse electromagnetic obstacle scattering, *Inverse Problems*, **24** (2008), 035018, 13 pp.

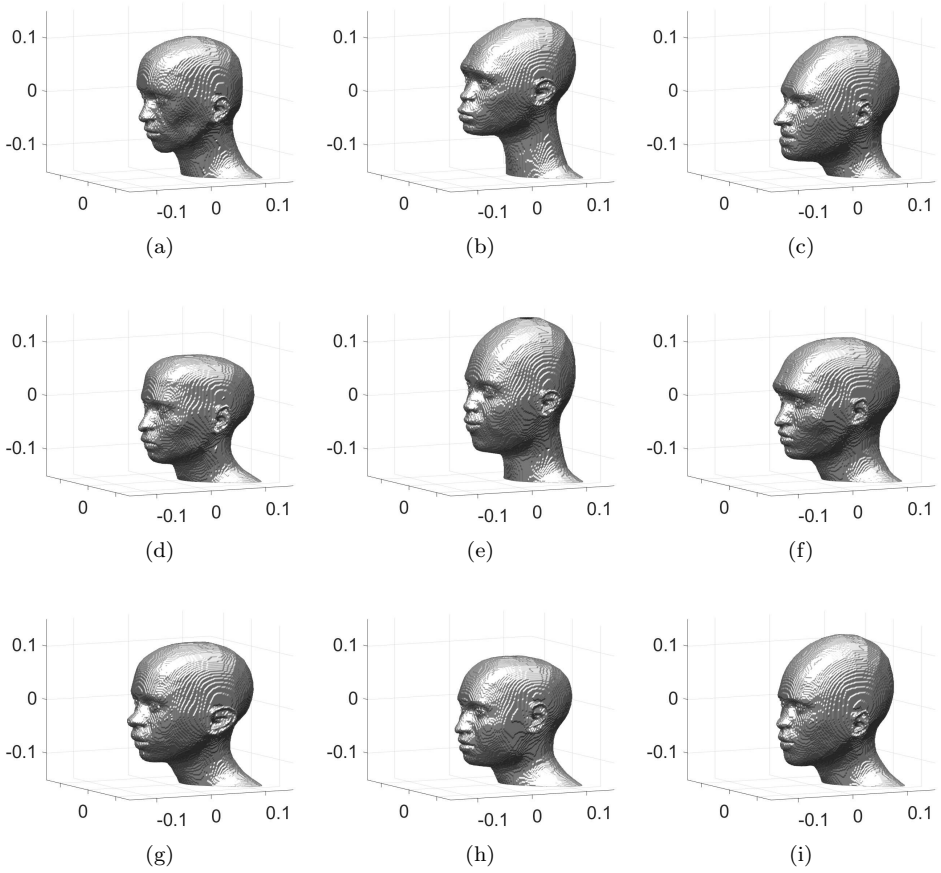

FIGURE 3. Isosurface plots of some random training head data with different characteristic values.

[8] H. Liu, L. Rondi and J. Xiao, Mosco convergence for $H(\mathrm{curl})$ spaces, higher integrability for Maxwell's equations, and stability in direct and inverse EM scattering problems, *J. Eur. Math. Soc. (JEMS)*, **21** (2019), 2945–2993.

[9] H. Liu, M. Yamamoto and J. Zou, Reflection principle for the Maxwell's equations and its application to inverse electromagnetic scattering problem, *Inverse Problems*, **23** (2007), 2357–2366.

[10] H. Liu and J. Zou, Uniqueness in an inverse acoustic obstacle scattering problem for both sound-hard and sound-soft polyhedral scatterers, *Inverse Problems*, **22** (2006), 515–524.

[11] T. Sauer and Y. Xu, On multivariate Lagrange interpolation, *Math. Comp.*, **64** (1995), 1147–1170.

[12] H. Seo, F. Cordier and N. Magnenat-Thalmann, Synthesizing animatable body models with parameterized shape modifications, *Proceedings of the 2003 ACM SIGGRAPH/Eurographics Symposium on Computer Animation. Eurographics Association*, (2003), 120–125.

[13] M. Takada and T. Esaki, Method and apparatus for measuring human body or the like, *U.S. Patent*, (1983), 406–544.

[14] G. Wang, F. Ma, Y. Guo and J. Li, Solving the multi-frequency electromagnetic inverse source problem by the Fourier method, *J. Differential Equations*, **265** (2018), 417–443.

[15] X. Wang, M. Song, Y. Guo, H. Li and H. Liu, Fourier method for identifying electromagnetic sources with multi-frequency far-field data, *J. Comput. Appl. Math.*, **358** (2019), 279–292.

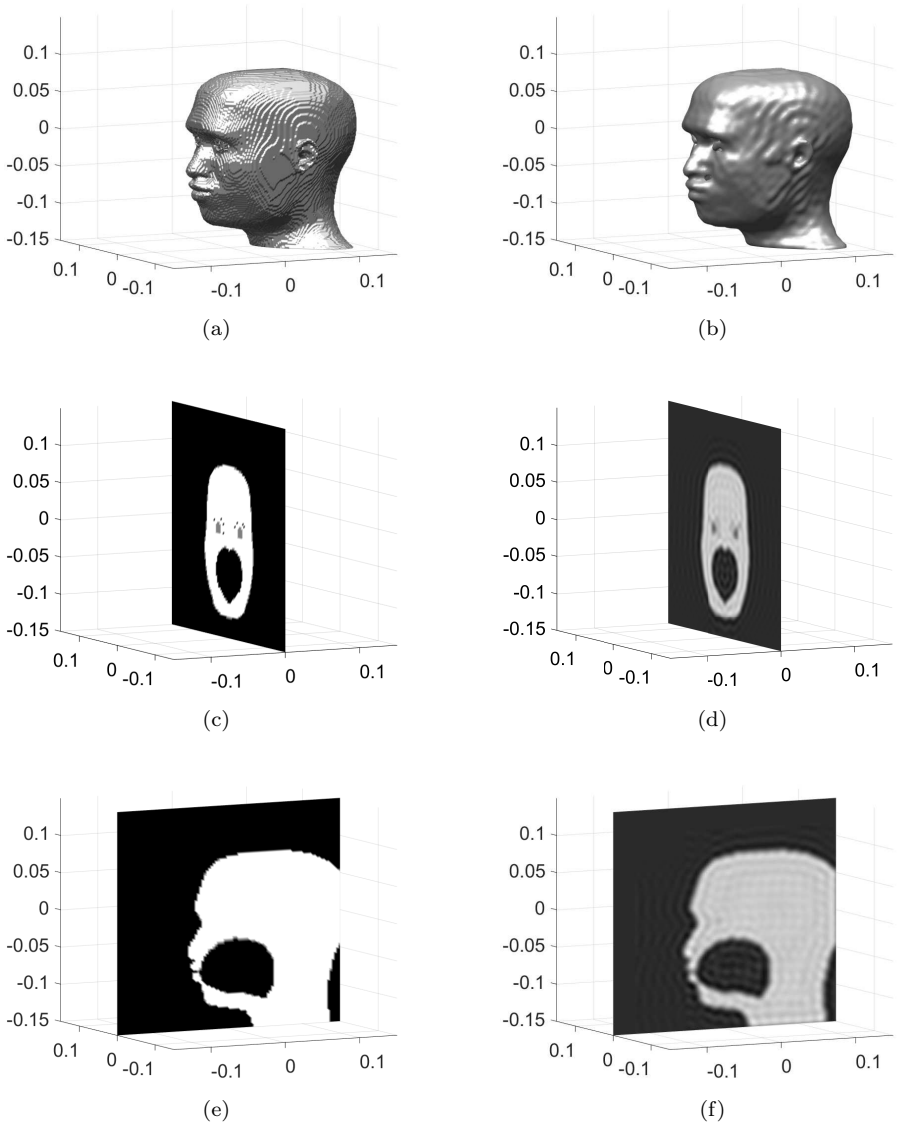

FIGURE 4. Plots of the exact and reconstruted head shapes with the given characteristic values. The left column: the exact head shapes, the right column: the reconstruted head shapes.

[16] D. Zhang and Y. Guo, Fourier method for solving the multi-frequency inverse source problem for the Helmholtz equation, *Inverse Problems*, **31** (2015), 035007, 30 pp.
[17] D. Zhang, Y. Guo, J. Li and H. Liu, Retrieval of acoustic sources from multi-frequency phaseless data, *Inverse Problems*, **34** (2018), 094001, 21 pp.
[18] D. Zhang, Y. Guo, J. Li and H. Liu, Locating multiple multipolar acoustic sources using the direct sampling method, *Commun. Comput. Phys.*, **25** (2019), 1328–1356.
[19] D. Zhang, F. Sun, Y. Guo and H. Liu, Unique determinations in inverse scattering problems with phaseless near-field measurements, *Inverse Problems and Imaging*, **14** (2020), 569–582.

[20] Make Human Community: Open Source tool for making 3D characters, Available from: http://www.makehumancommunity.org.

Received May 2020; revised May 2020.

E-mail address: 18481469@life.hkbu.edu.hk
E-mail address: ribbenlee@126.com
E-mail address: sheng_tingting@126.com
E-mail address: xcwang90@gmail.com